Supporting Information

Fast CO_2 hydration kinetics harm heterogenous, but benefit enzymatic CO_2 reduction catalysis

Samuel J. Cobb,[†] Vivek M. Badiani,[†] Azim M. Dharani,[†] Andreas Wagner,[†] Sonia Zacarias,[‡] Ana Rita Olivera,[‡] Inês A. C. Pereira[‡] and Erwin Reisner[†*]

[†]Yusuf Hamied Department of Chemistry, University of Cambridge, Lensfield Road, Cambridge CB2 1EW, U.K.

[‡]Instituto de Tecnologia Química e Biológica António Xavier, Universidade Nova de Lisboa, Av. da Republica, 2780-157 Oeiras, Portugal

*Corresponding Author: reisner@ch.cam.ac.uk

Table of Contents

Supplementary Text

Section 1: Carbonic Anhydrase Activity Assay

A Wilbur-Anderson assay[1] was used to measure the activity of CA in solution, verifying its activity as 3500 ± 570 WA U mg^{-1}. The assay was modified by adding the enzyme immobilised on a surface, as opposed to freely diffusing in solution. The enzyme was assumed to be quantitatively immobilised in the porous electrodes, as the surface area is sufficient to immobilise all the enzyme loaded (40 pmol) and for planar electrodes the surface was assumed to be saturated with enzyme, the loading of which was determined to be 4.3 pmol cm^{-2} (Extended Data Fig. 1), giving a total enzyme loading of 0.8 pmol on the 0.19 cm^2 electrode used. When enzyme loading was accounted for the enzyme displayed comparable activities in solution. While the average Wilbur Anderson unit activity measured for surface immobilised CA was consistently lower than when in solution, the values are within error. It must be considered that the apparent surface activity is limited by the mass transport of CO_2 to the surface, and H^+ to the pH meter that would be expected to give a rate lower than the V_{max} of the enzyme, this may explain the below error reduction in activity as opposed to any change in the activity of the enzyme. As such enzyme activities were assumed to be unaffected from the solution values.

CA Enzyme kinetics from Wilbur-Anderson assay

The nature of the Wilbur-Anderson assay means that getting enzyme turnover frequencies (TOFs) that can be used for inputting into a finite element model is not straightforward. Therefore, a 0D solution phase model was constructed in python using the ordinary differential equation integration (odeint) library from the open-source SciPy package and the Tkinter package was used to construct a graphical user interface for the model, allowing one to input their experimental parameters and plot how solution pH changes

with time without requiring coding experience. The model uses binary search to first iteratively solve for the amount of dissolved CO_2 in solution before using this concentration to iteratively solve for the enzyme's turnover frequency. This model is included as supporting information and includes a graphical user interface to allow simple calculation of CA parameters from solution assay results. The conditions for this work were as described in SI Table 4, representative of the assay.

CA was assumed to follow reversible Michaelis-Menten kinetics, with the rate as described in SI Eq. 1.

$$\nu = \frac{k_{cat,f}[CO_2].[E]/K_{m,f} - k_{cat,b}[HCO_3^-].[E]/K_{m,b}}{(1+\frac{[CO_2]}{K_{m,f}}+\frac{[HCO_3^-]}{K_{m,f}})} \quad \text{(Eq. 1)}$$

Where $K_{m,f}$ and $K_{m,b}$ were set to 8.3 and 32 mM, respectively,[2] with K_m being fairly invariant throughout the literature and also invariant on pH, although k_{cat} can vary significantly depending on the preparation and as such the Wilbur-Anderson assay was used to calculate the values of $k_{cat,f}$ and $k_{cat,b}$. The catalytic rates of CA have been shown to depend on the ionisation of a group with $pK_{a,e}$~7, this was described using SI Eqs. 2–3.[2]

$$k_{cat,f} = k^0_{cat,f}\frac{K_{a,e}}{[H^+]+K_{a,e}} \quad \text{(Eq. 2)}$$

$$k_{cat,b} = k^0_{cat,b}\frac{[H^+]}{[H^+]+K_{a,e}} \quad \text{(Eq. 3)}$$

The equilibrium of CO_2, HCO_3 and H^+ are related by the equilibrium constant (K_{eq}), a value unchanged by the presence of enzyme. Therefore a modified Haldane relation can be derived to link $K_{m,f}$,$K_{m,b}$,$k_{cat,f}$ and $k_{cat,b}$ (SI Eq. 4).[2] Therefore $k_{cat,f}$ and $k_{cat,b}$ can be derived together.

$$\frac{k^0_{cat,f}}{K_{m,f}}.\frac{K_{m,b}}{k^0_{cat,b}}.K_{a,e} = K_{eq} \quad \text{(Eq. 4)}$$

The solution kinetics for uncatalysed CO_2 hydration and buffer kinetics were as described in SI Table 6, from this the enzyme rate that matches the activity observed in the assay could be found. When no enzyme was present the experimental blank time of 94(.3) ± 8 s was used to calculate a [CO_2] of 11.545 mM in this assay (SI Fig. 1). The enzyme kinetics described by SI Eqs. 2–4 were added to the model to simulate the addition of CA, with the [E] set from the assay conditions (0.033 µM, 0.005 mg in 5.005 ml) and iterately solved for $k^0_{cat,f}$ and $k^0_{cat,b}$ to match the experimental assay time of 5.06 s. This gave an enzyme activity of 3500 WA U mg^{-1} and a TOF of 49000 s^{-1} (SI Fig. 1) to give the values for enzyme kinetics in SI Table 2 that were used with SI Eqs. 1–4 to describe CA in the FEM in all cases going forward.

Section 2: Finite Element Modelling

Enzyme Finite Element Model

A 2D axisymmetric tertiary current distribution model was constructed in COMSOL Multiphysics 5.6 to represent the enzyme system of interest. The model is designed to represent enzyme activity through well-defined analytical expressions that can calculate the enzyme catalytic current dependent on: applied potential, pH, solution composition and substrate concentrations.

This is unlike a purely mass transport derived model that relies on experimental currents to infer on the environment within the porous electrode, and allows the accurate prediction of experimental currents from a model that requires no knowledge of the outcome of experiments.[3] The enzyme kinetic expressions are fixed for all experiments with a specific enzyme, and only solution conditions are changed. This approach is therefore predictive of current densities and the effect of changes in the solution can be correlated with experimental values as the simulation takes no direct input from the outcomes of the experiment. This allows the unequivocal demonstration that the changes in solution properties studied herein can give the experimentally observed current responses as these currents have not been assumed in

the simulation and are calculated with the same enzyme kinetic properties for all experiments. This gives internal validation of the hypotheses observed. Furthermore, this allows the in-silico optimisation of the solution properties beyond the initial test data sets for the highest predicted current densities. This can then be validated with experiment and allows the design of optimal catalytic enzyme solutions systems in-silico as experimentally inaccessible parameters can be used to inform rationally on the system design.

Simulation Geometry

The inclusion of turbulent convection from stirring means explicitly describing the entire solution volume is exceedingly computationally expensive and therefore a stagnant diffusion layer was used. This consists of 3 domains (SI Fig. 2):

1- An infinite elements domain with a fixed concentration boundary that represented bulk solution

2- A diffusion layer that varied in thickness dependent on the model conditions as described below

3- A porous electrode with geometry and porosity determined from scanning electron microscopy (SEM) and the Bruggeman equation used to describe the change in system properties due to the porosity

1- Infinite Elements Domain

An Infinite elements domain represents an infinitely large domain, and in this case represents bulk solution, within this domain the concentrations of all species are fixed at their starting values. As such no depletion or concentration of species occurs in this domain and it acts as an infinitely large solution volume as is assumed in experiment beyond the diffusion layer. This is combined with a concentration boundary condition on the interface between domains

1 and 2, where the species concentration on the interface is fixed to the initial values at time zero. This represents the edge of the stagnant diffusion layer

2- Solution Domain

Fick's Law for a stagnant layer (SI Eq. 5) was used with a redox mediator (2 mM $[Fe(CN)_6]^{4-/3-}$) to calculate the diffusion layer thickness for the stirred electrochemical cell.

$$i_{lim} = nFAD\frac{c}{\delta} \quad \text{(Eq. 5)}$$

This current averaged over the last 100 s (29.2 ± 0.6 μA cm^{-2}, SI Fig. 9) gave a diffusion layer thickness of 500 ± 10 μm when there is no catalytic current, but gas evolution, in particular in the case of enzymatic HER, can enhance the mass transport of species to and from the surface by increasing convection.[4] This was included in the finite element model (FEM) using a current dependence of the diffusion layer thickness (SI Fig. 10). To generate this, the diffusion length was assumed to have a contribution from convection (k_{conv}) and bubbles (k_{bubble}) (SI Equation 6–7). In this case, due to the lack of bubble formation, k_{bubble} was assumed to be 0 and therefore k_{conv} could be calculated to be 1.15 x 10^{-3} cm s^{-1}.

$$\delta = \frac{D_i}{k_{MT}} \quad \text{(Eq. 6)}$$

$$k_{MT} = k_{conv} + k_{bubble} \quad \text{(Eq. 7)}$$

K_{bubble} was calculated using an approximate bubble diameter (d_b) of 250 μm (SI Eq. 8). Two Sherwood's numbers were calculated (SI Eqs. 9–11), Sh_1 relating to the effects of bubble break off where fluid immediately replaces the departing bubble for which we use the Rousar correlation and Sh_2 which describes the combined effects of bubble growth and wake flow, for

which Vogt's correlation (Θ < 0.5) was used (Eq. S11). The bubble coverage (Θ) was assumed to be 0.25 and the ratio of inactivated electrode area below a nucleated bubble as it grows (R_a/R) was assumed to be 0.75.

$$k_{bubble} = \frac{Sh_{bubble} + D_i}{d_b} \quad \text{(Eq. 8)}$$

$$Sh_{bubble} = (Sh_1^2 + Sh_2^2)^{0.5} \quad \text{(Eq. 9)}$$

$$Sh_1 = \sqrt{\frac{12}{\pi}} Re_G^{0.5} Sc^{0.5} \Theta^{0.5} \quad \text{(Eq. 10)}$$

$$Sh_2 = \frac{2}{\sqrt{5}} Re_G^{0.5} Sc^{0.34} \left(1 - \frac{\sqrt{8}}{3} \frac{R_a}{R} \Theta^{0.5}\right)(1 + \Theta) \quad \text{(Eq. 11)}$$

The Reynolds and Schmidt numbers for gas evolution are described by SI Eq. 12 and 13, where the volume flux of gas evolution (related to the current passed) has been used to calculate the Reynolds number and the kinematic viscosity of water (0.01 $m^2 s^{-1}$)

$$Re_G = \frac{j}{nF} \frac{RT}{P} \quad \text{(Eq. 12)}$$

$$Sc = \frac{\nu}{D} \quad \text{(Eq. 13)}$$

K_{bubble} is highly dependent on the applied potential, and therefore the diffusion layer thickness changes with current. A plot of diffusion layer thickness *vs* current density was generated based on the equations above (SI Fig. 10). This was used to calculate the apparent diffusion layer thickness for each experiment, a value that was held constant during the measurement due to the complexities of moving meshes. The system current that determined the diffusion coefficient was taken from experiment.

The diffusion coefficients of species in water at 25 ^{o}C are listed in SI Table 7. The values have been corrected for viscosity using the Stokes-Einstein equation. The protonated and deprotonated forms of MES were assumed to have the same diffusion coefficients.

Solution Thermodynamics & Kinetics

In the FEM model, the solution reactions were represented by the equations and equilibrium constants (K) in SI Table 5. These equilibria were subject to the effects of ionic strength as described by the Davies equation (SI Eq. 14). All equilibria were written in terms of activities, where $a=\gamma_i c_i$ and γ was calculated using the Davies equation. The activity of water was assumed to be constant at 1.

$$\log \gamma_i = -Az_i^2 \left(\frac{\sqrt{I}}{1+\sqrt{I}} - 0.3I\right) \qquad \text{(Eq. 14)}$$

The thermodynamics of bulk solution still hold within the diffusion layer, and the same governing equations and constants are used within this domain, but due to its finite size not all reactions can be assumed to be at equilibrium within it. While MES buffer was assumed to be diffusion limited and therefore always at equilibrium, the slow kinetics of CO_2 hydration mean such an assumption is not valid. As such the rate constants ($k_{f,0}$) in SI Table 6 were used for the bicarbonate system. The constants stated are the rate constants at 0 M ionic strength and the Davies equation was used to modify these rate constants to reflect the

change of the equilibrium constant with ionic strength, such that $K=k_{f,0}/k_r$ meaning k_f remained constant and k_r was adjusted

3- *Porous Electrode Domain*

The electrode radius was 2.5 mm (SI Fig. 8). The electrode thickness and porosity were taken from SEM imaging (Extended Data Fig. 3). The porous electrode domain was assumed to be 9 µm thickness and randomly close packed. An electrode volume fraction of 0.64 and electrolyte volume fraction of 0.36 was used, the maximally jammed limit of a randomly close packed structure.[5] This is in reasonable agreement with observations from SEM and would be expected from a spin coated electrode. Effective transport parameters for diffusion, electrode and electrolyte conductivity were calculated using the Bruggeman equation.[6]

The electrode specific surface area (surface area/volume, a_v) was approximated using an assumption of close packed cubic particles with point contacts between them. As such the specific surface area could be approximated using SI Eq. 15.

$$a_v = \frac{surface\ area}{volume} \times volume\ fraction = \frac{6l^2}{l^3} \times 0.64 \qquad \text{(Eq. 15)}$$

For a particle of side length 46 nm the specific surface area is 8.35×10^7 m^{-1}, giving an electrode surface area of 139 cm^2.

In addition, the porous electrode has additional reactions from the solid electrode component, below.

Porous electrode solution reactions

To represent chemical reactions within the solution in the porous electrode the same solution kinetics and thermodynamics were used as in the solution domain above (SI Table 5–6). Rates were multiplied by a factor to represent the reduced solution volume within this domain (0.36 solution volume). To describe CA enzyme immobilisation within the porous electrode SI Eq. 1–4 were used to describe the interconversion of CO_2 and HCO_3^- in addition to those in the solution domain, due to CA being only located within the electrode.

Enzyme electrode current density

The enzyme current was represented using SI Eqs. 16–17

$$i_{H2ase} = i_{PD} \times a_{pH,rel} \quad \text{(Eq. 16)}$$

$$i_{FDH} = i_{PD} \times a_{pH,rel} \times a_{[CO_2],rel} \quad \text{(Eq. 17)}$$

Where SI Eq. 16 represents the H_2ase catalytic current density and SI Eq. 17 the FDH catalytic current density with respect to the geometric electrode area.

I_{PD} represents the potential dependent current of the enzyme, using the analytical description previously reported[7] for the reductive case using an EC_r mechanism, where E is a redox transformation of the active site and C_r is a reversible chemical reaction, with a dispersion of k_0 values that could be attributed to a variation in the immobilisation orientation that leads to a distribution of electron transfer distances from the surface. The values (SI Table 8) for Fdh and H_2ase were taken from literature where available or fitted to representative CVs. $I_{red,lim,m}$ is the molar limiting current for the enzyme, and as such is multiplied by the enzyme loading

within the porous electrode (20–50 pmol) to give the limiting current used in the potential dependence.

In SI Eqs. 16–17 $a_{pH,rel}$, $a_{[CO2],rel}$ and $a_{buffer,rel}$ are values between 0 and 1 that represent the relative activity of the enzyme dependent on the solution pH, CO_2 concentration and buffer composition, respectively. These previously reported dependencies were determined from solution assays, where other factors, such as mass transport or electron transfer limitations, are minimised and as the enzyme dependence can be measured free of convolution. The $a_{pH,rel}$ used for H_2ase and FDh is shown in SI Fig. 11 where the points represent the experimental data and the lines a linear interpolation that was used to give the relative activity in the model.

$a_{co2,rel}$ for FDh was assumed to follow Michaelis-Menten kinetics, with K_m determined from solution assay to be 0.420 mM by Oliveira et. al (SI Fig. 12).[8,9] No comparable dependence of substrate concentration on H_2ase activity is used as H^+ is the substrate and as such any dependence is included with $a_{pH,rel}$.

These expressions combine to give a comprehensive description of the enzyme activity within this system, including consideration of numerous experimental factors that could be responsible for changes in enzyme activity and therefore current. These currents are used within the porous electrode domain, below, to give the rates of consumption and generation of reactants and products within the porous electrode domain.

Porous Electrode Volumetric current

The electrode surface area is irrelevant to the current observed, this is due to enzyme being assumed to be quantitatively loaded as the quantity of enzyme loaded is insufficient to saturate the large surface area of the porous electrode. As such within the range of enzyme loadings

used in this study the electrode area does not affect the current, and an increased electrode surface area leads to a lower specific current density (the current density considering the surface area within the volume of the porous electrode as opposed to the geometric surface area of the electrode).

As the specific surface area of the electrode and the enzyme surface density directly cancel, the volumetric current density (I_v) does not depend on the surface area within the electrode and purely the amount of enzyme immobilised within that volume. The enzyme is assumed to be homogenously distributed within the porous electrode volume. This volumetric current density (I_v, SI Eq. 18) that is included within the model- representing the current density observed within each volume element of the porous electrode from the enzyme current SI Eqs. 16–17.

$$i_v = \frac{i_{enz}}{V_{element}} \quad \text{(Eq. 18)}$$

This represents the current density passed within each element and is calculated based on the enzyme activity within that element of the simulation that is dependent on the properties of that element.

Electrode Reaction Stoichiometry

The overall stoichiometry (ν) of the reactions given in Table S9 for the respective enzymes, H_2ase and FDh was combined with the volumetric current density, above, to give the rate (R) of species consumption and generation within each element (SI Eq. 19). The reactions were assumed to occur with 100% Faradaic efficiency.

$$R_i = \frac{-\nu_i i_v}{nF} \quad \text{(Eq. 19)}$$

Mesh

The equations and relationships above were discretised on a mesh such as those shown in SI Fig. 13, which is finest where the reaction gradients are highest– within and at the surface of the porous electrode. Both the potential and the concentrations were described by linear Lagrange elements. The discretised equations were solved in COMSOL Multiphysics 5.6. Accuracy of the calculated solutions was confirmed when no appreciable change was observed using a finer mesh or higher tolerances with the solver.

Au Finite Element Model

A 1D finite element model was constructed in COMSOL Multiphysics 5.6 to represent electrocatalysis on a planar Au surface. This was closely based on the model by Zhang et al.[10] and includes apparent kinetics rates for CO_2R and HER. Fully describing the catalytic processes on Au is complex, with numerous rate equations required for both CO_2R and HER due to the multiple mechanisms and proton donors. Building a complete model containing the kinetics and thermodynamics of all processes is not currently possible, as the individual kinetic rates cannot be determined from experiment. Instead, two rate equations describe the apparent rates of CO and H_2 formation. These equations do not represent the rates of individual physical processes occurring on the electrode surface, but provide a good representation of the overall rates and therefore can give a good insight into the mass transport and solution processes coupled to these kinetic expressions. The kinetic rates were

first set to give a good agreement with the electrocatalysis on Au in the absence of CA. The rate constants used were similar to those found by Zhang et al.[10] and described the system across all the potentials used. CA kinetics were then added to the solution domain with no further modifications and the response of the system studied to assess the effect of adding CA in solution to Au electrocatalysis.

Solution Domain

The solution domain was constructed as above for the enzymatic case, however both CO_2R and HER were gas evolving reactions, affecting the apparent diffusion layer thickness (SI Fig. 10). The solution reaction thermodynamics and kinetics were unchanged in the absence of CA (SI Table 5–6). Species diffusion coefficients used in this domain were identical to the enzymatic case (above, SI Table 7). When CA was present the enzyme rates in SI Table 2 were used in SI Eqs. 1–4 to include this contribution to the solution rates.

Electrode Current Density

The electrode kinetics took the form of the apparent rate equations for CO_2R to CO (SI Eqs. 20–21) and HER (SI Eq. 22) used by Zhang et al. that can appropriately describe the overall rates of reaction.[10]

$$j_{CO} = 2FR_f k^{ap}_{f,CO_2}(E).[CO_2] \quad \text{(Eq. 20)}$$

$$k^{ap}_{f,CO_2}(E) = k^{ap}_{CO_2}(E).e^{\left(\frac{-0.5FE}{RT}\right)} \quad \text{(Eq. 21)}$$

$$j_{H_2} = 2FR_f k^{ap}_{HCO_3^-}.e^{\left(\frac{-\alpha^{ap}_H FE}{RT}\right)}[HCO_3^-] \quad \text{(Eq. 22)}$$

The parameters used in SI Eqs. 20–22 were taken from readily available experimental data where possible. The roughness factor (R_f) was determined to be 15 from electrochemical surface area measurements using Au oxide stripping.[10] Further kinetic parameters were determined by fitting to experimental k^{ap}_{HCO3-} was determined to be 5×10^{-8} cm s^{-1} and α^{ap}_H to be 0.17, these values were close to those found previously to describe the apparent

kinetics.[10] The value of k^{ap}_{CO2} was varied with potential to match the experimental result in an identical manner to Zhang et al.,[10] these values are tabulated in SI Table 10.

Electrode stoichiometry

The stoichiometry (v) of CO_2R and HER given in SI Table 11 for Au was combined with the current density from SI Eqs. 20 and 22 for CO_2R and HER respectively, to give the rate (R) of species consumption and generation within each element using SI Eq. 19 (above).

Supporting Figures

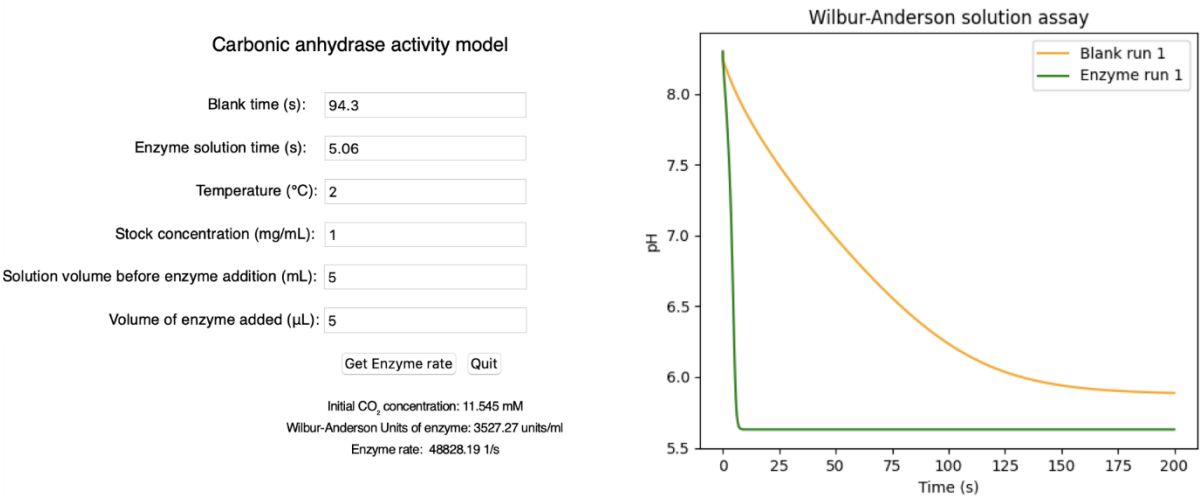

Figure 1. *Screenshot of graphical user interface of script used to calculate CA enzyme rates from experimental Wilbur-Anderson assay. Plot shows simulated pH from enzyme free blank and enzyme containing solution assays.*

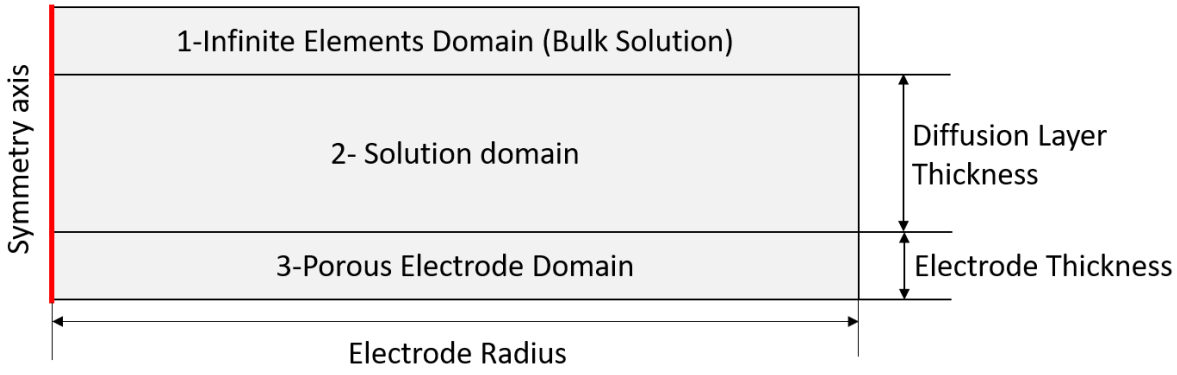

Figure 2. *Schematic description of FEM geometry (not to scale)*

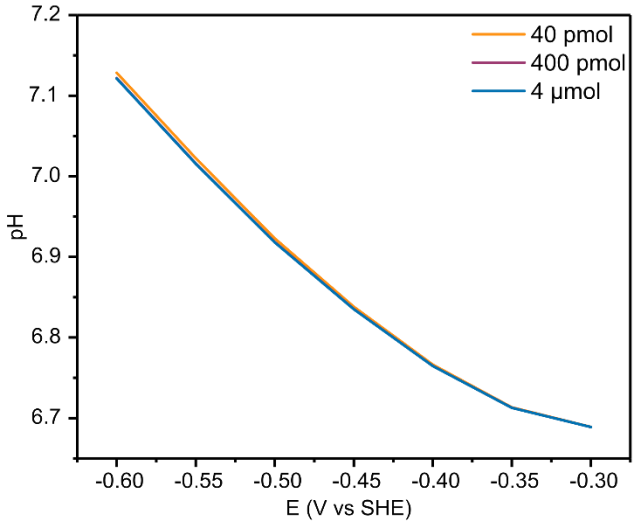

Figure 3. *Simulation of mesoITO|Fdh (50 pmol) in CO_2 purged 0.1 M $KHCO_3$ + 0.05 M KCl (pH 6.67) at steady state (t= 360 s) with 40 pmol – 4 µmol of CA, demonstrating the minimal effect of increased CA concentrations on the local environment as the kinetics are sufficiently fast that the system has reached its thermodynamic equilibrium.*

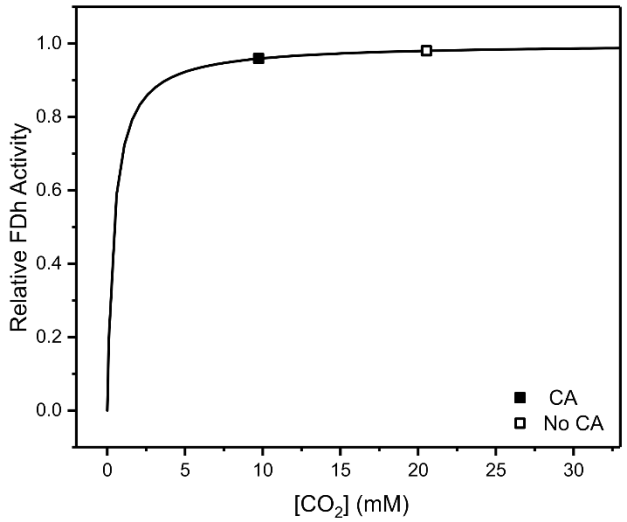

Figure 4 *Effect of CO_2 concentration on CO_2R activity. The line represents the enzyme Michaelis-Menten kinetics determined from solution assay (K_M = 0.420 mM)[29] and the points are the simulated local CO_2 concentrations used in this work from Extended Data Figure 8(20 pmol H_2ase+ 50 pmol FDh) at −0.6 V vs SHE in the presence (filled points) and absence (empty points) of CA (40 pmol). Conditions: 0.1 M $KHCO_3$ (CO_2 purged), T= 20°C*

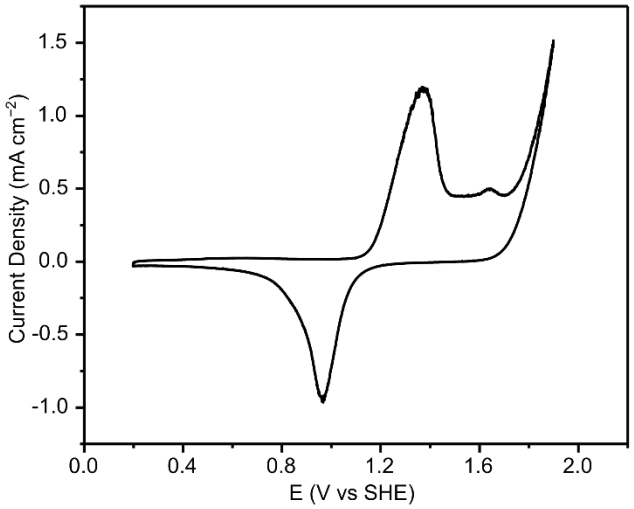

***Figure 5**. Current Averaged Cyclic Voltammogram of Au electrode in 50 mM H_2SO_4 for electrochemical surface area measurement. The reduction peak at ~ –1 V was integrated giving a charge passed of 3.52 mC cm^{-2} and a roughness factor of 15.*[10] T= 20°C.

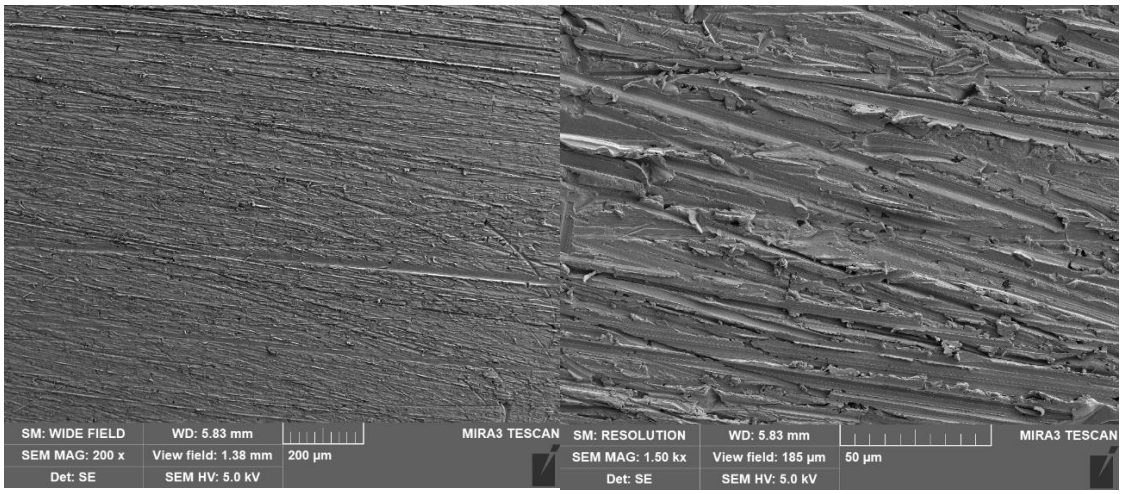

***Figure 6**. SEM images of Au electrode surface demonstrating the surface roughness. SEM HV: 5.0 kV; WD: 5.83 mm, Detector: secondary electron.*

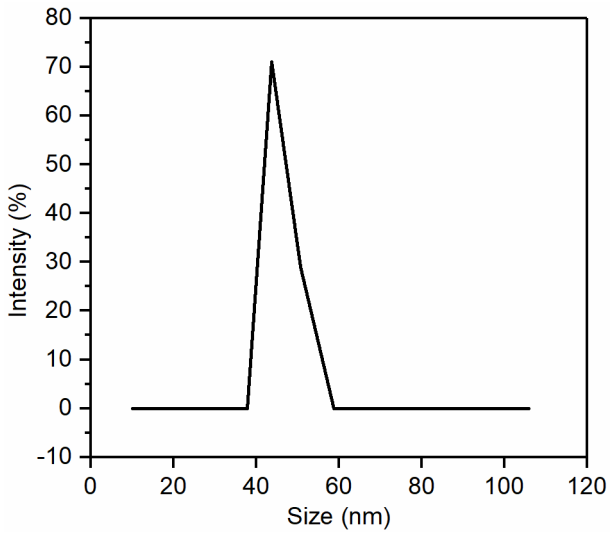

Figure 7. *ITO nanoparticle size distribution determined by Dynamic Light Scattering. Conditions: 0.05 mg mL^{-1} homemade ITO dispersed in 10% (v/v) acetic acid/water. The average particle size was determined to be 45.6 nm ± 1.4 nm.*

Figure 8. *Photograph of a wired electrode.*

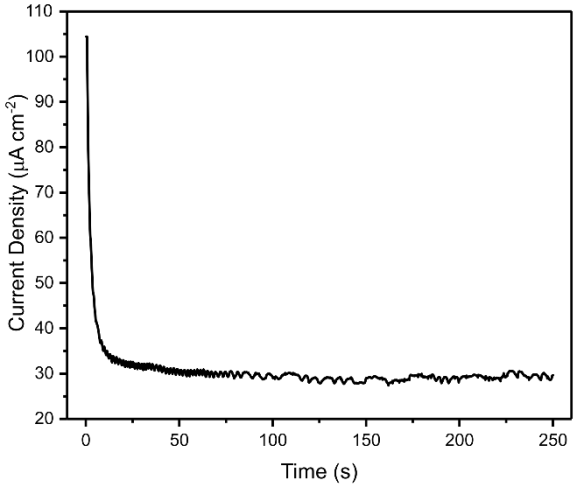

Figure 9. *Chronoamperometry to determine the limiting current density of 2 mM $[Fe(CN)_6]^{4-}$ in the cell, geometry and convection conditions used for all electrochemical experiments in this work. E_{app}= +0.4 V vs SHE (E_0= 0.16 V vs SHE).* T= 20°C.

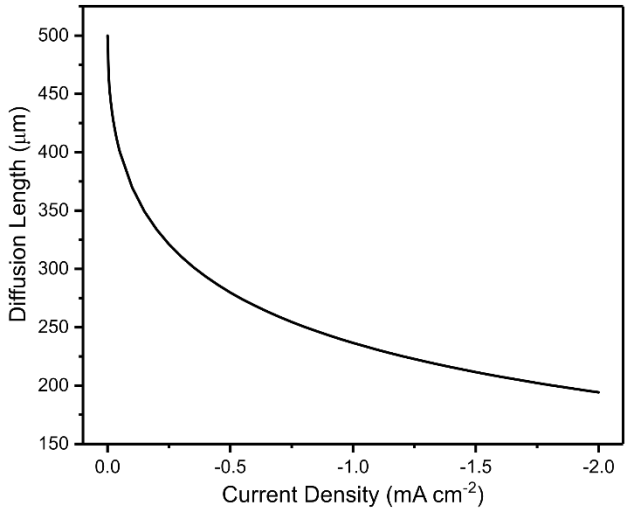

Figure 10. *Effect of convection from H_2 gas evolution on the diffusion layer thickness in a stagnant diffusion layer model. This dependency was derived from Eqs. 5–13 above.*

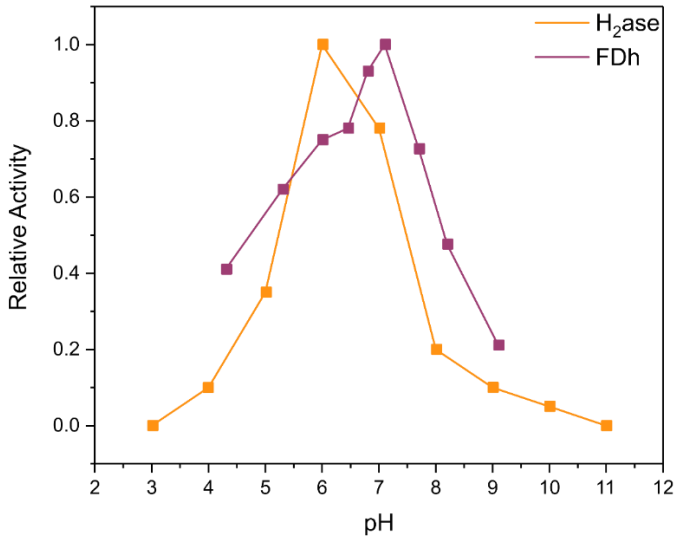

***Figure 11**. Enzyme activity dependence on pH for H_2ase (orange) and FDh (purple), data taken from Marques et al. and Oliveira et al., respectively.[8,9] Points represent experimental data and lines a linear interpolation used for FEM.*

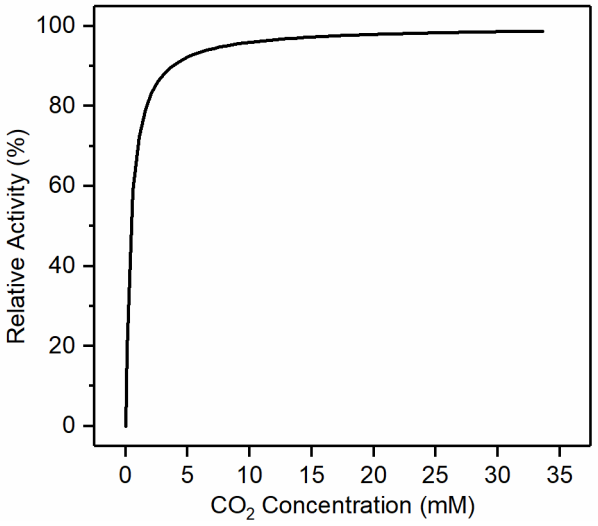

***Figure 12**. Enzyme activity dependence on CO_2 concentration for FDH, K_m= 0.420 mM, data taken from Oliveira et al.[8]*

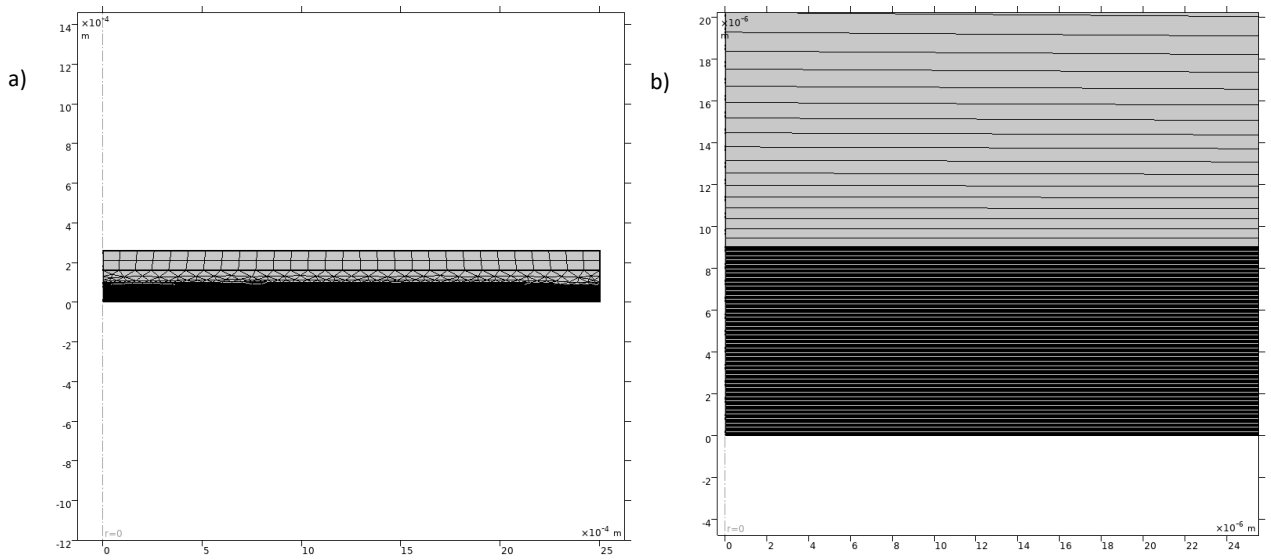

***Figure 13**. Example mesh used for enzyme finite element simulations. Left: full domain; right: zoom-in to porous electrode at r = 0.*

Supporting Tables

Table 1. *Effect of atmosphere gas composition on H_2ase activity*

Atmosphere	Rate (s^{-1})
1 atm N_2	6557±121
1 atm CO_2	6997±73

Table 2. *Kinetic Parameters of CA used for FEM modelling.*

Parameter	Value
$k^0_{cat,f}$	49000 s^{-1}
$k^0_{cat,b}$	17170 s^{-1}
K_e	8×10^{-8} M
$K_{m,f}$	8.3 mM
$K_{m,b}$	32 mM

Table 3. *Current densities and product quantifications at highest overpotentials.*

$KHCO_3$	MES	CO_2	pH	CA	H_2ase	FDh	E	J_{tot}	J_{H2}	J_{CO}	J_{HCOO-}	FE_{H2}	FE_{CO}	FE_{HCOO-}
mM	mM	mM			pmol		V vs SHE			$\mu A\ cm^{-2}$			%	
100	X	32	6.67	X	X	X	-0.65	-35	-32	n.d.	n.d.	91	–	–
100	X	32	6.67	40	X	X	-0.65	-13	n.d.	n.d.	n.d.	-	–	–
100	X	32	6.67	X	20	X	-0.65	-210±37	-180± 58	n.d.	n.d.	85±9	–	–
100	X	32	6.67	40	20	X	-0.65	-540±42	-470± 46	n.d.	n.d.	87±7	–	–
100	X	32	6.67	X	X	50	-0.6	-255±56	n.d	n.d	-240±77	–	–	94±6
100	X	32	6.67	40	X	50	-0.6	-500±49	n.d	n.d	-490±47	–	–	97±6
50	50	32	6.45	X	X	X	-0.65	-23	-19	n.d.	n.d.	82	–	–
50	50	32	6.45	40	X	X	-0.65	-18	-n.d.	n.d.	n.d.	-	–	–
50	50	32	6.45	X	20	X	-0.65	-450±43	-400±48	n.d.	n.d.	88±6	–	–
50	50	32	6.45	40	20	X	-0.65	-680±44	-570±35	n.d.	n.d.	84±9	–	–
50	50	32	6.45	X	X	50	-0.6	-470±14	n.d	n.d	-460±11	–	–	97±4
50	50	32	6.45	40	X	50	-0.6	-600±110	n.d	n.d	-560±120	–	–	94±9
X	132	X	6.45	X	X	X	-0.65	-28	-24	n.d.	n.d.	86	–	–
X	132	X	6.45	40	X	X	-0.65	-11	-n.d.	n.d.	n.d.	-	–	–
X	132	X	6.45	x	20	X	-0.65	-680±18	-590±16	n.d.	n.d.	87±8	–	–
X	132	X	6.45	40	20	X	-0.65	-720±51	-620±100	n.d.	n.d.	86±6	–	–

Table 4 *Solution Conditions for Wilbur-Anderson Assay Simulation at t=0.*

Parameter	Value
$[CO_2]$	11.545 mM
[Tris-H]	8.7 mM
$[Tris^-]$	3.3 mM
$[HCO_3^-]$	0 mM
$[CO_3^{2-}]$	0 mM
$pK_{tris,0c}$	8.72
pH	8.3
T	2 °C

Table 5*. Equilibrium constants of reactions used in the finite element model. The equilibrium constants are defined in terms of activity. Water is always assumed to be activity 1.*

Equation	K_0
$CO_2 + OH^- \rightleftharpoons HCO_3^-$	4.57×10^{-7}
$HCO_3^- + OH^- \rightleftharpoons CO_3^{2-}$	5.01×10^{-3}
$MESH + OH^- \rightleftharpoons MES^-$	5.37×10^{-7}
$2H_2O \rightleftharpoons H^+ + OH^-$	10^{-14}

Table 6. *Forward ($k_{f,0}$) and reverse ($k_{r,0}$) rate constants for chemical reactions in solution that cannot be considered to be diffusion limited.*

Equation	$k_{f,0}$ $M^{-1}\ s^{-1}$	$k_{r,0}$ s^{-1}
$CO_2 + OH^- \rightleftharpoons HCO_3^-$	1.25×10^4	2.73×10^{-4}
$HCO_3^- + OH^- \rightleftharpoons CO_3^{2-}$	1.07×10^5	2.15×10^4

Table 7 *Diffusion coefficients of species in solution at 25 ^oC.*

Species	Diffusion Coefficient $m^2\ s^{-1}$
CO_2	1.48×10^{-9}
HCO_3^-	9.25×10^{-10}
CO_3^{2-}	7.25×10^{-10}
OH^-	5.27×10^{-9}
H^+	7.8×10^{-9}
MESH	8.2×10^{-10}
MES^-	8.2×10^{-10}
H_2	4.58×10^{-9}
$HCOO^-$	1.45×10^{-9}

Table 8 *Enzyme electrode kinetic and thermodynamic parameters for H_2ase and FDh.*

	H_2ase	FDh
$k_{red,lim}$	8280[9]	315[8]
$k_{ox,lim}$	2430[9]	1310[8]
K^0_{OR}	1	1
$\beta_{d,0}$	1	4
E_0 (V vs RHE)	0	-0.11

Table 9 *Enzyme electrode reaction stoichiometry.*

	H_2ase	FDH
n_e	2	2
OH^-	2	1
H_2	1	0
CO_2	0	−1
$HCOO^-$	0	1

Table 10 *Values of k^{CO}_{app} across the potential range*

E vs SHE	k^{CO}_{app}
−0.79	1.43×10^{-13}
−0.84	1.43×10^{-13}
−0.89	1.43×10^{-13}
−0.93	1.08×10^{-13}
−0.98	7.48×10^{-14}
−1.06	2.98×10^{-14}
−1.15	9.86×10^{-15}

Table 11 *Au Electrode reaction stoichiometry.*

	CO_2R	HER
n_e	2	2
OH^-	2	0
H_2	0	1
CO_2	−1	0
CO	1	0
HCO_3^-	0	−2
CO_3^{2-}	0	2

Supporting References

1. Wilbur, K. M. & Anderson, N. G. Electrometric and Colorimetric Determination of Carbonic Anhydrase. *J. Biol. Chem.* **176**, 147–154 (1948).

2. Steiner, H., Jonsson, B. & Lindskog, S. The Catalytic Mechanism of Carbonic Anhydrase. *Eur. J. Biochem.* **59**, 253–259 (1975).

3. Suter, S. & Haussener, S. Optimizing mesostructured silver catalysts for selective carbon dioxide conversion into fuels. *Energy Environ. Sci.* **12**, 1668–1678 (2019).

4. Burdyny, T. *et al.* Nanomorphology-Enhanced Gas-Evolution Intensifies CO2 Reduction Electrochemistry. *ACS Sustain. Chem. Eng.* **5**, 4031–4040 (2017).

5. Torquato, S., Truskett, T. M. & Debenedetti, P. G. Is random close packing of spheres well defined? *Phys. Rev. Lett.* **84**, 2064–2067 (2000).

6. Tjaden, B., Cooper, S. J., Brett, D. J., Kramer, D. & Shearing, P. R. On the origin and application of the Bruggeman correlation for analysing transport phenomena in electrochemical systems. *Curr. Opin. Chem. Eng.* **12**, 44–51 (2016).

7. Fourmond, V. & Léger, C. Modelling the voltammetry of adsorbed enzymes and molecular catalysts. *Curr. Opin. Electrochem.* **1**, 110–120 (2017).

8. Oliveira, A. R. *et al.* Toward the Mechanistic Understanding of Enzymatic CO_2 Reduction. *ACS Catal.* **10**, 3844–3856 (2020).

9. Marques, M. C. *et al.* The direct role of selenocysteine in [NiFeSe] hydrogenase maturation and catalysis. *Nat. Chem. Biol.* **13**, 544–550 (2017).

10. Zhang, B. A., Ozel, T., Elias, J. S., Costentin, C. & Nocera, D. G. Interplay of Homogeneous Reactions, Mass Transport, and Kinetics in Determining Selectivity of the Reduction of CO_2 on Gold Electrodes. *ACS Cent. Sci.* **5**, 1097–1105 (2019).

End of Supporting Information